Article

Intracochlear Scala Media Pressure Measurement: Implications for Models of Cochlear Mechanics

Sushrut S. Kale[1,*] and Elizabeth S. Olson[1,2]

[1]Department of Otolaryngology and [2]Department of Biomedical Engineering, Columbia University, New York, New York

ABSTRACT   Models of the active cochlea build upon the underlying passive mechanics. Passive cochlear mechanics is based on physical and geometrical properties of the cochlea and the fluid-tissue interaction between the cochlear partition and the surrounding fluid. Although the fluid-tissue interaction between the basilar membrane and the fluid in scala tympani (ST) has been explored in both active and passive cochleae, there was no experimental data on the fluid-tissue interaction on the scala media (SM) side of the partition. To this aim, we measured sound-evoked intracochlear pressure in SM close to the partition using micropressure sensors. All the SM pressure data are from passive cochleae, likely because the SM cochleostomy led to loss of endocochlear potential. Thus, these experiments are studies of passive cochlear mechanics. SM pressure close to the tissue showed a pattern of peaks and notches, which could be explained as an interaction between fast and slow (i.e., traveling wave) pressure modes. In several animals SM and ST pressure were measured in the same cochlea. Similar to previous studies, ST-pressure was dominated by a slow, traveling wave mode at stimulus frequencies in the vicinity of the best frequency of the measurement location, and by a fast mode above best frequency. Antisymmetric pressure between SM and ST supported the classic single-partition cochlear models, or a dual-partition model with tight coupling between partitions. From the SM and ST pressure we calculated slow and fast modes, and from active ST pressure we extrapolated the passive findings to the active case. The passive slow mode estimated from SM and ST data was low-pass in nature, as predicted by cochlear models.

INTRODUCTION

The cochlea is a fluid-filled tube separated into compartments by an elastic partition, commonly termed the cochlear partition (CP), that houses the organ of hearing. Due to coupling between the inertia of the fluid and restoring force provided by the CP, stapes motion creates a fluid-pressure/tissue-displacement wave that travels down the cochlea and is known as the cochlear traveling wave (TW) (1,2). The cochlear TW travels much slower than sound in fluid, and the TW mode of sound propagation is often termed as the slow wave or the slow mode. In addition to this 1) slow mode, there is 2) a compressional (sound pressure) mode that is in phase with the in/out plunging motion of the stapes, and fills the cochlea almost uniformly (3), as well as 3) evanescent modes that exist in the basal region near the oval and round windows, and decay rapidly toward the apex (4–6). Like the compressional mode, the evanescent mode is coupled with stapes motion without any traveling delay, thus both compressional and evanescent modes are fast modes. The compressional mode is symmetric, whereas the slow and the evanescent modes are antisymmetric across the CP (Fig. 1). These pressure modes exist due to physical and geometrical properties of the cochlea and hence are present even in passive, linear cochleae.

These are fundamental building blocks of passive cochlear mechanics, which forms the substrate for active mechanics. Recent studies have discussed these different modes and their relation to cochlear excitation (5,8).

In most cochlear models only the slow mode is considered, because the evanescent modes are relatively small in amplitude and diminish rapidly with distance from the windows, and the compressional mode does not drive motion of the CP. Classic models consider a two-compartment (scala tympani (ST) and scala vestibuli (SV) + scala media (SM) as a single compartment) cochlea separated by an elastic partition. These are single partition models. In a one-dimensional (1D) version of the model only longitudinal variations are present. This model predicts an equal magnitude and opposite phase (antisymmetric) slow mode between the two compartments, with symmetric fast mode added to satisfy the boundary condition at the round window and stapes (3). Classic two-dimensional (2D) and three-dimensional (3D) models still assume an antisymmetric slow mode in two compartments but the slow mode can vary radially (3D models) and vertically (2D and 3D models) (Fig. 2 B, z direction) (7). Cochlear models generally predict that the (passive) slow-mode pressure is low-pass in nature (2,3,7,10).

In active models slow-mode pressure tuning and nonlinearity is typically brought about by a net negative real part in the CP's mechanical impedance—negative resistance,

---
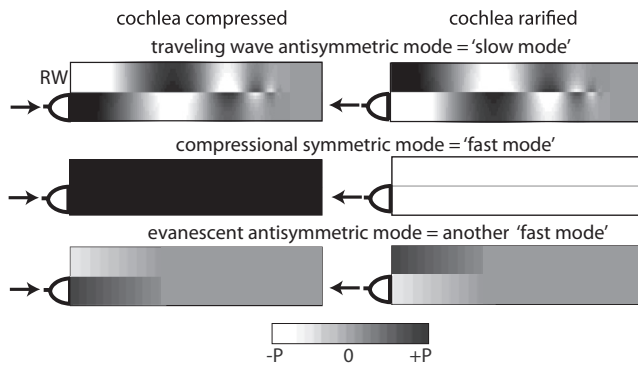
FIGURE 1 Cartoon of pressure modes in the cochlea. Response to a rather low frequency is shown for illustration, so that the traveling wave mode travels down most of the cochlear length. Many cochlear models only consider the antisymmetric traveling wave mode (*top panels*, 2D example shown) but this is not adequate to satisfy the boundary conditions, particularly the boundary condition at the round window, where the pressure will be ~0 (*atmospheric*). Peterson and Bogert's 1D model solved this by adding a symmetric compressional mode (*middle panels*). With 2D and 3D cochlear models, evanescent modes are also present (*bottom panels*) that taper off exponentially from the region of the cochlear windows (7). (They would also vary vertically although this is not included in the simple cartoon.)

or local stimulus enhancement (11). In more detailed models, this enhancement is accomplished by incorporating electromechanical feedback from outer hair cells into an underlying passive model (12,13).

The next step in complexity allows for coupled motion of two elastic partitions, corresponding approximately to the tectorial membrane (TM) and basilar membrane (BM) (14–16). In these two-partition models, the TW (slow-mode) pressures and motions in ST and SM + SV are no longer necessarily antisymmetric. The slow mode on the BM is coupled to the fluid in the ST, and the slow mode on the TM is coupled to the fluid in the SM. The slow modes on the TM and BM will be very similar (and approximately antisymmetric) if there is tight coupling between

the TM and BM, but can be different if the TM and BM are only loosely coupled. These two-partition models are especially compelling now that TM waves are well established (17,18).

In active cochleae intracochlear pressure in ST is tuned and nonlinear (e.g., (19,20)) The ST pressure close to the BM shows much similarity to BM motion measured with techniques such as laser interferometry (21–24). Both the ST pressure (Fig. 3) and BM motion findings can be summarized as follows. 1) The magnitude peaks at the best frequency (BF) and scales nonlinearly with the sound pressure level. 2) The phase of the response relative to middle ear or ear canal (EC) pressure shows delays of several cycles in the peak frequency region, indicating dominance of slow-mode pressure. 3) The peak is followed by a nearly flat, plateau region at higher frequencies. (The magnitude of the plateau is relatively larger in pressure than motion, compared to the magnitude at frequencies below the plateau.) The high-frequency amplitude plateau is accompanied by a nearly flat phase that can jump in integer multiples of 2π with sound level, indicating a fast mode that dominates the slow mode at lower frequencies at higher sound levels. 4) The magnitude response often shows a notch above the peak where the phase transitions from slow mode dominated to fast mode dominated. 5) At high sound pressure levels (SPLs) magnitude and phase responses look similar to postmortem responses, i.e., broad peak and fewer cycles of delay. These findings have informed our understanding of cochlear nonlinearity and active mechanics, provided evidence of fast and slow modes within the cochlea, and provided a degree of validation for the classical theories of passive cochlear mechanics.

However, there were no experimental data regarding the pressure close to the TM in SM. This gap becomes more serious as TM waves become firmly established and two-partition models more fully developed. To address this gap, in this study we measured intracochlear pressure in
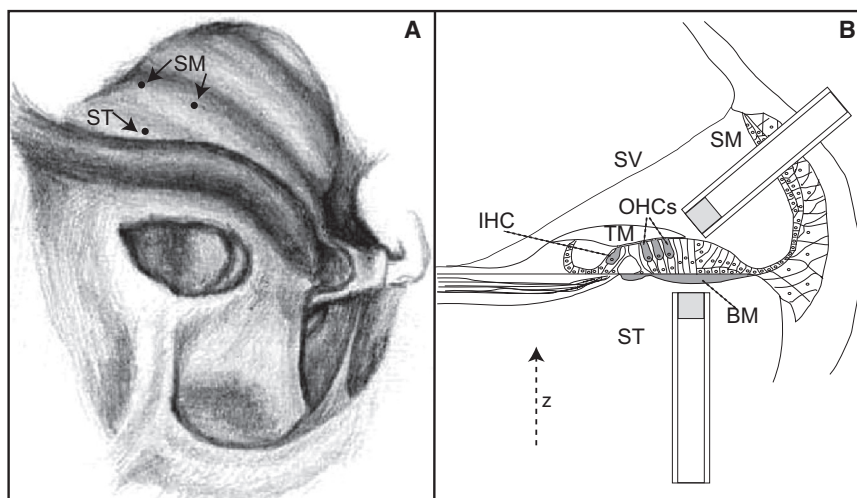
FIGURE 2 Approach for SM and ST pressure measurements. (*A*) Sketch of the gerbil cochlea. Black dots indicate the locations of cochleostomies for SM and ST pressure measurements. (*B*) Sketch of the cross section of the CP indicating estimated sensor positions. IHC, inner hair cell; OHCs, outer hair cells; ST, scala tympani; SM, scala media; SV, scala vestibule; TM, tectorial membrane; BM, basilar membrane.
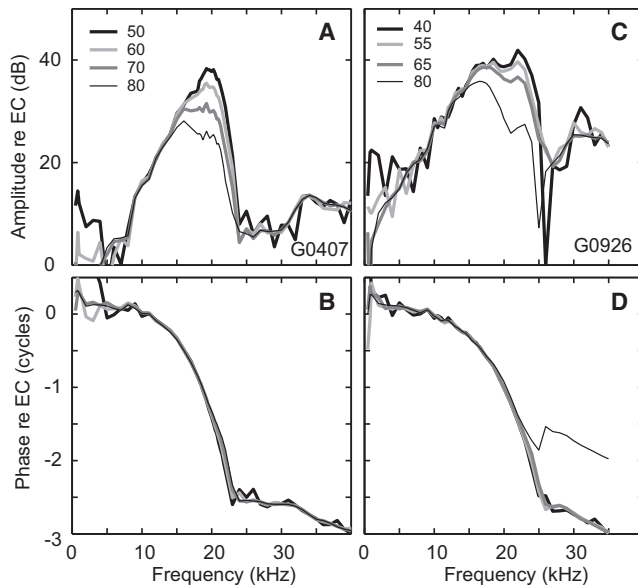
FIGURE 3   ST pressure relative to pressure in the EC measured from two animals (*A* and *B*, gerbil G0407; *C* and *D*, gerbil G0926) using new single-mode, smaller sensor (see text for details). The pressure was measured within 10 μm of the BM. For these measurements the SM lateral wall was not opened and the EP is therefore expected to be normal and the cochleae were active (*nonlinear*).

SM, close to the TM, followed in some preparations by ST pressure at the BM.

The ~100 μm opening into SM that was required to make the measurements caused the cochlea to lose its activity, thus the experimental aspect of the study is of passive cochlear mechanics. We used our SM + ST pressure data at the TM and BM to compute fast and slow waves at the TM and BM, based on the quantitative definitions provided in previous work (3). We will see that with this analysis the slow mode at the partition is basically low-pass in nature. This finding agrees with the low-pass shape of passive slow mode in cochlear models, and is contrasted with the bandpass character of the passive ST pressure. Furthermore, we discuss how our results relate to BM motion measurements that showed evidence of fast modes in motion. Finally, we extrapolate our findings to predict the slow mode in the active cochlea.

MATERIALS AND METHODS

Experimental methods

The experiment protocol was approved by Columbia University's Institutional Animal Care and Use Committee (IACUC). Young adult mongolian gerbils (*Meriones unguiculatus*) weighing 50–65 g were sedated with ketamine and anesthetized with sodium pentobarbital. Supplemental doses of sodium pentobarbital were given to maintain a surgical plane of anesthesia. Body temperature was monitored using a rectal probe and was maintained at ~37°C with an electric heating pad. 0.5 cc saline solution was injected intraperitoneal every 2 h. for hydration. The animal's head was glued to a small goniometer using dental cement. The left pinna was removed to

expose the EC. Sound was delivered using a RadioShack speaker via a flexible plastic tube. An ultrasonic Sokolich microphone calibrated the sound within ~2 mm of the tympanic membrane. Single tones were delivered and data collected using a Tucker Davis Technologies DAQ system and MATLAB (The MathWorks, Natick, MA).

Although all experiments commenced in vivo, in a few cases the animals expired before data collection. Due to the passive mechanics under study, we continued the experiments. In our experience, passive mechanical responses are not changed greatly within a few hours postmortem. Previously, two studies have reported significant downward shifts of the frequency of the passive peak and traveling wave phase excursion, 7–16 h postmortem (25) and 1–7 days postmortem (26). Thus, we expect some degree of downward shifting of response features in our data that were taken ~3–4 h postmortem. However, these shifts were not obvious in our grouped data. We note postmortem cases in the featured data.

Intracochlear pressure sensors

Intracochlear pressure was measured using microfiberoptic pressure sensors. Construction and operation of similar sensors has been described previously (27,28). Briefly, the sensors are constructed by threading fiber optic into a narrow glass capillary tip with a gold-plated polymer membrane termination. The fiber is fixed at a distance ~50 μm from the membrane. Light exits the fiber to reflect off the membrane and returns to the fiber, and some fraction of it reenters the core and is transmitted back to a photodetector. Pressure-induced motion of the membrane modulates the amount of light returning to the fiber core. Our previous studies used sensors with tips of outer diameter ~150 μm, later reduced to ~125 μm. Those sensors used multimode fiber optic (we call them the multimode sensors). In multimode fibers the inner core is typically 50 μm in diameter and the light is an LED. The outer diameter of the fiber optic is 125 μm when purchased and is reduced by etching in hydrofluoric (HF) acid for all sensor types. The multimode sensors were successful in measuring pressure in the ST far from and close to the BM and in the SV near the stapes. The ST and SV spaces are larger than the SM and more accessible. To be able to measure the SM pressure, we developed, to our knowledge, new smaller sensors made with single-mode fiber optic that has a much narrower inner core (9 μm). The outer diameter of these single-mode fibers starts at 125 μm and was reduced with HF acid to 35 μm to thread them into narrow sensor capillary tips, with ID/OD 40/80 μm. For the single-mode sensors, a superluminescent diode was the light source. The single-mode sensors were constructed and worked in a way similar to the multimode sensors. The sensors were calibrated in water and air. These transducers are linear and have a nearly flat frequency response through at least 50 kHz. With 1 s of signal averaging they showed intracochlear sensitivity down to stimulus levels of ~30 dB SPL in the EC.

The sensors are calibrated before and after experiments. During some measurements, the sensor's output voltage shifted phase by 180° and/or showed a vertical shift in calibration magnitude (Volts/Pascal), based on sensor calibrations done before and after the experiment. Thus, the sensor's calibration during measurements could be uncertain. We have presented the pressure data with the phase and sensitivity shown as reliably as possible, and this required applying frequency-independent amplitude shifts and 180° phase shifts in some data sets (where stated). The multimode sensors suffer from phase flipping too, but rarely (29). Both phase flipping and calibration magnitude shifts were more prevalent with the single-mode sensors. This is probably due to the light returning to the much smaller inner core (9 μm versus 50 μm diameter for the multimode sensors.) It is worth emphasizing that calibration shifts occur in a frequency-independent manner, so do not influence the measurement of frequency response. We also emphasize that to make the measurements in SM, the smaller (single-mode) sensors were necessary. More information on the sensors, including their component parts, calibration examples, and discussion of temporal bone measurements in which multimode sensor stability is highly controlled, is in (27).

Pressure measurements

Surgery was performed to expose the ventral bulla, which was opened to expose the cochlea. For ST measurements, a small hole (~100 μm in diameter) was hand-drilled into ST in the basal turn. Using a micropositioner, the sensor was slowly advanced into ST in 1-μm steps. The sensor signal was monitored on the oscilloscope to detect when the sensor membrane touched the BM. The fluid pressure was measured within 10 μm of the tissue and also at several locations as the sensor was retracted over a range of ~150 μm. In ST, the sensor membrane was almost perpendicular to the BM as shown in the sketch (Fig. 2 B).

To perform SM pressure measurements we had to go through the lateral wall including stria vascularis and in these measurements it was not possible to preserve endocochlear potential. For SM pressure measurements, the lateral wall was exposed after drilling a hole in the SM bone (~100 μm in diameter). A small electric cautery with a 10-μm diameter tip was used to deliver a short current pulse that created a clean opening through the lateral wall. All the SM pressure data presented in this work represent passive, linear cochlear mechanics, probably due to loss of endocochlear potential. In eight animals, SM pressure was measured from a basal location near the 20–22 kHz BF place. In five animals, SM pressure was measured from a relatively apical location (see Fig. 2 A, *black dots* for locations). In three animals, intracochlear pressure was measured sequentially from both ST and SM and in two of these three animals the SM and ST pressure was measured at roughly the same longitudinal location (Fig. 2 A). Intracochlear pressure was measured only in SM in 10 animals and only in ST in three animals. Making a small hole in SM did not alter the passive cochlear mechanics as was confirmed in two animals by making ST pressure measurements before and after making the SM hole. In one experiment, the SM sensor was sealed in place by dental cement and the SM pressure measured after resealing the hole was similar to that measured with the open SM-hole. It is also notable that in previous studies holes in SV near the stapes did not alter cochlear mechanics, even active mechanics (19).

Stimuli

Stimuli were pure tones ranging in frequency from 0.2 to 30–40 kHz. Because the purpose of this study was to investigate passive cochlear mechanics from both sides of the CP, most of the data were collected at 70–85 dB SPL. However, for a few ST pressure measurements, pure tones were presented at sound levels ranging from 40 to 80 dB SPL to facilitate the comparison between this data set and previously published data. In these cases ST data were collected first and nonlinear, active cochlear mechanics were observed in ST pressure. For every experiment, at the beginning of data collection, stimuli were presented with wider frequency sampling to assess gross features of intracochlear pressure. Following this initial data set, stimulus frequencies were closely spaced (200–240 Hz apart) over a wide region (~4 kHz) surrounding peaks and notches. Due to such fine frequency sampling, the phase excursions corresponding to the notches observed in the data were not a result of inadequate phase unwrapping.

RESULTS

ST pressure measured with new smaller sensors was nonlinear and sharply tuned

Fig. 3 shows ST pressure, normalized by the EC pressure, measured within 10 μm from the BM, in two different animals using the single-mode sensors (i.e., new, smaller sensors). ST pressure peaked near 20–22 kHz and showed nonlinearity over the 17–25 kHz range. Phase responses showed that the ST pressure consisted of a slow, TW mode that varied rapidly with frequency (dominant in the peak region) and a fast mode, which was relatively flat

with frequency (dominant in the 25–40 kHz region, Fig. 3, B and D). At the transition between the two regions a deep notch could develop, indicating destructive interference between the two modes (Fig. 3 C). In animal 0926, at the high SPL, the phase leveled off one cycle above that at low SPLs (Fig. 3 D). This indicates that the fast mode started to dominate at a lower frequency for the higher SPL. This is a familiar finding from ST pressure (19) and BM motion results (21). The data in Fig. 3, although not among the most nonlinear, best ST data sets (19,30) are consistent with previous measurements of ST-pressure tuning, nonlinearity and phase, and show that the smaller, single-mode sensor can reliably be used for intracochlear pressure measurements.

SM pressure showed a pattern of peaks and notches

Fig. 4 shows summary data of the SM pressure measured close to the sensory tissue (within 8–10 μm) in the more basal location in eight animals (Fig. 4, A and B), and the relatively more apical location in five animals (Fig. 4, C and D). The two longitudinal locations were ~1 mm apart, ~2 and 3 mm from the basal end of the cochlea. In both locations, the responses were characterized by a fairly flat region at lower frequencies, a notch, and another fairly
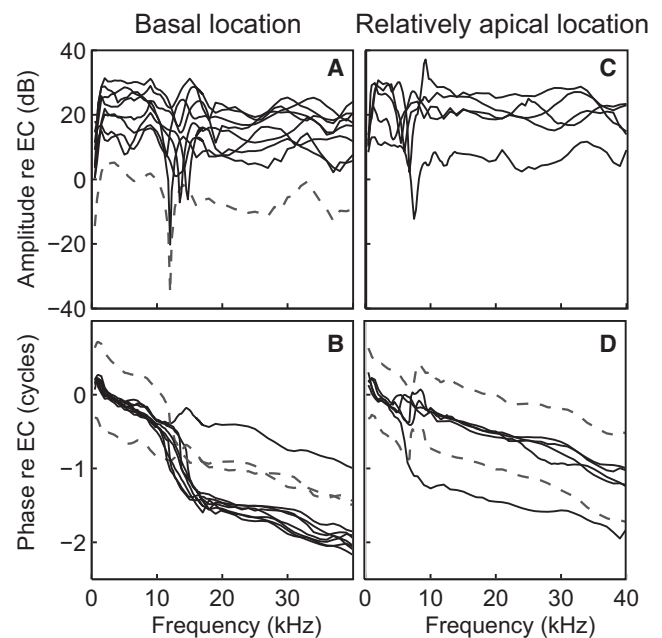
FIGURE 4 SM pressure measured from 13 animals, collected 8–10 μm from the sensory tissue. (A and B) In eight animals, data were collected from the basal region. (C and D) In five animals, data were collected from a relatively apical region. In four of these data sets, the sensor flipped phase by a half cycle (180°) (*dashed lines* in B and D). During one experiment the sensor sensitivity dropped substantially (*dashed lines* in A) and those data are replotted as a solid black line with a 15 dB boost. Data with 180° sensor phase flip has been replotted with phase correction as solid black lines.

flat region above the notch, with amplitude slightly less than the lower frequency flat region. The amplitude of the pressure relative to the EC pressure (pressure gain) varies by ~10–20 dB in the range of ~20 dB in both SM and ST. However, in Fig. 4 A there is one outlier with much smaller gain, but the same frequency shape (*dashed line*). This spread of magnitude is to some degree due to an uncertainty in sensor calibration, as noted in the Materials and Methods section. Fortunately, when the sensor sensitivity changed it was a vertical shift. Hence, this case was replotted as a solid line in Fig. 4 with a flat 15 dB boost, which was approximated by comparing before and after experiment sensor calibrations. Fig. 4 reaffirms that the frequency structure is not affected by the uncertainty in the sensor sensitivity.

The frequency range of the notch was different in the basal measurement location (12–16 kHz, Fig. 4 A) and the apical measurement location (5–9 kHz, Fig. 4 C). As explained later, this notch was the manifestation of the summing of fast- and slow-mode pressure and hence varied with the measurement location, because the peak of the slow-mode pressure varies with the location.

In both locations the phase of the responses underwent a transition in the region of the amplitude notch. The phase transition could be an excursion greater than a full cycle. Such large phase excursions indicate that the slow-mode pressure was dominant through an extensive frequency range. In other cases, the phase transition reversed and did not complete a full cycle. Likely, the sensor was not positioned in a way that allowed it to pick up the slow mode well in these cases. (This will be discussed further, in Fig. 7 below). In four cases the phase was offset by 180° from the majority of the data (*dashed lines* in Fig. 4, B and D), and this is most certainly due to the calibration problem described previously. In these cases the phase has been flipped back in analysis (replotted as *solid lines* in panels B and D) and these are the more reliable presentation of the pressure phase. As this figure makes clear, 180° phase corrections and vertical shifts in magnitude are sometimes necessary preliminary steps in data analysis. In the remaining figures these shifts have been applied when necessary.

Fig. 5 shows SM pressure from two animals, measured at the two different longitudinal locations (a subset of the data of Fig. 4) to highlight the similarities and differences in the responses in the two regions. The basal location measurement (Fig. 5, A and B) was made from a location that would correspond to a BF of ~20 kHz in an active, nonlinear cochlea. This is based on our prior measurements from ST at the same longitudinal location, which consistently had a peak of ~20–22 kHz at low sound levels and a peak at ~14–16 kHz at a high sound level. The relatively apical measurement (Fig. 5, C and D), came from a location ~1 mm apical, where the CP turns to exit the first basal turn. To access this location, the SM hole was made medial to the stapes, where the cochlea almost disappears into the bone (see Fig. 2 A for the measurement locations). Similar
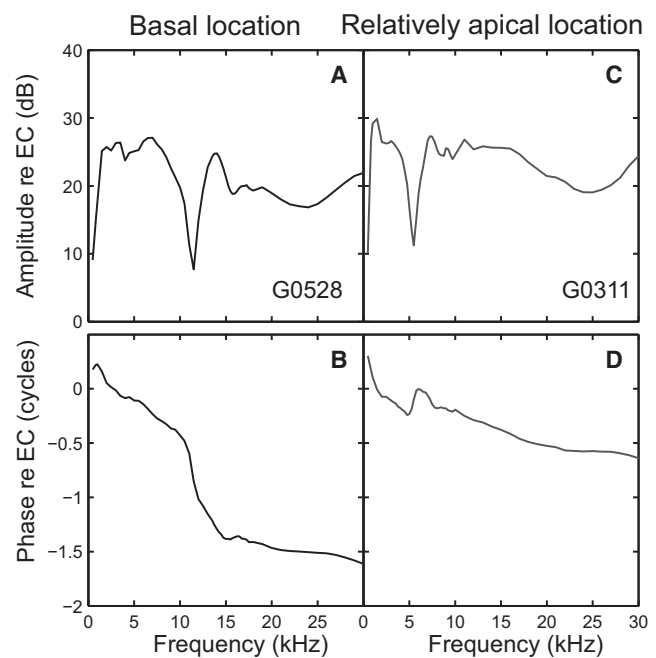
FIGURE 5 Two individual curves from the family of SM pressure data in Fig. 3 are replotted here to emphasize that the prominent notch occurs at a lower frequency in the relatively apical location. (*A* and *B*) Relatively basal location, gerbil G0528 (data taken postmortem). (*C* and *D*) Relatively apical location, gerbil G0311.

to ST pressure (shown in Fig. 3), the SM pressure close to the BM showed a rapidly varying phase, indicative of a slow mode in the BF region. The SM pressure magnitude showed a sharp notch whose frequency varied with the location of measurement. At frequencies above the notch the magnitude dropped 5–10 dB compared to below it. As shown in Fig. 4, this pattern of notches was consistent in all the SM pressure measurements. Such notches and corresponding phase variations indicate the summing of fast and slow pressure modes (Fig. 3 C and e.g., (19)).

In three experiments it was not possible to get very close and perpendicular to the CP due to where the cochleostomy was located and the angle of the approach. SM pressure measured in these experiments was approximately flat with frequency, without a notch, and resembled SV pressure (e.g., Fig. 5 in (28)). These SV pressure-like data underscore the need to measure the pressure close to the sensory tissue to study the slow mode and the interaction of the pressure modes. In both ST and SM the slow mode was undetectable in pressure measurements made far from the sensory tissue.

ST and SM pressure measurements from the same animal unraveled the pressure modes on the CP

Fig. 6 shows SM and ST pressure measured close to the sensory tissue in the same animal. Two examples are
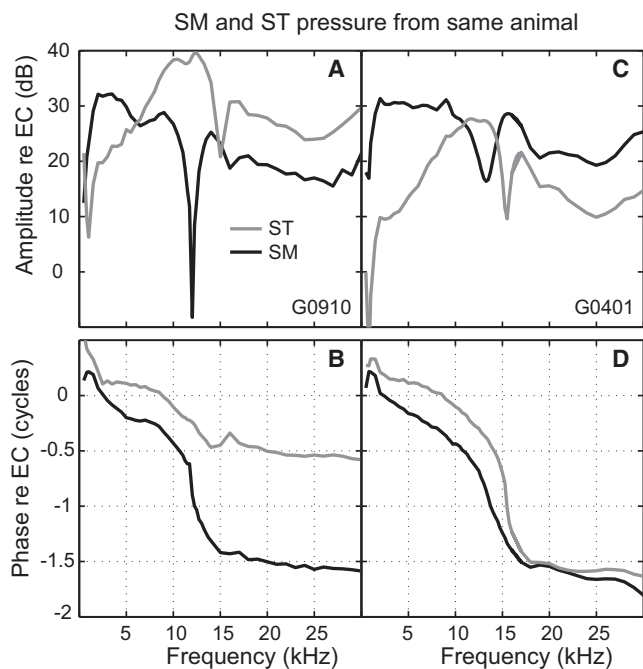
FIGURE 6 SM and ST pressure measured from the same animal. Data from two animals (*A* and *B*, gerbil 0910; *C* and *D*, gerbil 0401) are shown. Black lines indicate magnitude and phase of SM pressure and gray lines indicate the magnitude and phase of ST pressure. Both SM and ST pressure were measured within 10 μm of the sensory tissue. (*A* and *B*) Postmortem data from gerbil G0910. (*C* and *D*) In-vivo data from gerbil G0401.

shown, both from the relatively basal location with active CF ~20 kHz. Because all these data were taken after opening the SM, the pressure measurements represent passive linear cochleae. The ST pressure was measured after collecting the SM data and it resembled the passive data collected postmortem in previous studies (e.g., Fig. 8 in (19), Fig. 3 in (30)). This leads us to believe that the SM hole did not significantly alter the passive mechanics of the CP. SM and ST pressures were measured at approximately the same longitudinal location but from the opposite sides of the CP (Fig. 2 *A*).

The ST pressure showed a prominent peak around 15 kHz, which is the expected passive peak frequency for this location (corresponding to a peak of 20–22 kHz in an active cochlea.) At frequencies below the ST peak, ST pressure was smaller than SM pressure, which was relatively flat. The ST pressure peak was abruptly followed on the high frequency side by a notch. The SM pressure also displayed a prominent notch, as already noted in Figs. 4 and 5, and the SM notch occurred at a frequency in the middle of the ST peak. In the Discussion section, we show that the notch frequency location is predicted in a simple model of fast- and slow-mode vector summation. Regarding the phase, at the lowest frequencies the results were varied, likely due to the low amplitudes and influence of the holes. At frequencies of a few kHz the phases settled down and both SM and ST led the EC pressure slightly, a result that

is similar to our wealth of ST pressure data, and SV pressure data near the stapes (e.g., (19,20,28,30)). (At frequencies well below a location's BF, SM pressure is expected to be similar to SV pressure.) The consistency of the sub-BF phase results with this broad set of previously published data (taken with the multimode pressure sensors) further validates the 180° phase correction applied to four data sets presented in this study. At high frequencies, the phases were also similar between ST and SM—this can be interpreted as the fast mode, which in a classic model is symmetric: equal in amplitude and phase in the two fluid compartments. However, in our results the SM pressure amplitude was usually slightly larger than the ST amplitude. This might be due to calibration uncertainty, and the SM and ST amplitudes might actually be equal in the HF plateau region, as the classic Peterson and Bogert theory (3) predicts. On the other hand, the difference might be actually present, and due to an evanescent mode (6) as shown here in Fig. 1. Olson (19) also found SV pressure to usually be a few dB larger than ST pressure in the fast-mode frequency plateau. We will comment on this further in the Discussion section. Finally, in the broad frequency region of the ST peak from ~5 to 15 kHz, there was ~1/2 cycle difference between SM and ST phases. This is as predicted in the classic theory of the antisymmetric slow mode of single partition cochlear models (2,3).

Variation in SM pressure with change in sensor location in axial direction

Fig. 7 shows the variation in SM pressure as the sensor was retracted after touching the tissue. As the sensor retracted, the notch magnitude and phase varied. Because the fast mode is believed to be nearly spatially invariant, the changes within the notch region likely reflect the spatial variation of the slow-mode pressure. Closest to the tissue, (*black curve* in Fig. 7, *A* and *B*, G0603), we observed a shallow notch, a small peak, and rapid phase variation, thus the slow wave seems to be dominating the pressure at the closest location. However, in Fig. 7, *C* and *D*, G0318, closest to the tissue (*black line*), we observed only a shallow notch with a small phase excursion. As the sensor moved back 30 μm, a notch developed in the amplitude and the corresponding phase showed a steep excursion through a full cycle. Thus, with G0318, the slow mode was more dominant at that location than it was at the location closest to the tissue. We speculate that in G0603, when closest to the tissue, the sensor was close to the lateral side of the organ of Corti (OC, see sketch in the top row, *left panel*) and that this location had a robust TW. In contrast, we speculate that in G0318 (*right panel*), when closest to the tissue, the sensor was near a more medial part of OC and that this region had a smaller TW motion. The slow mode pressure is related to tissue motion and the absence of a dominant slow mode at the tissue in G0318 suggests that
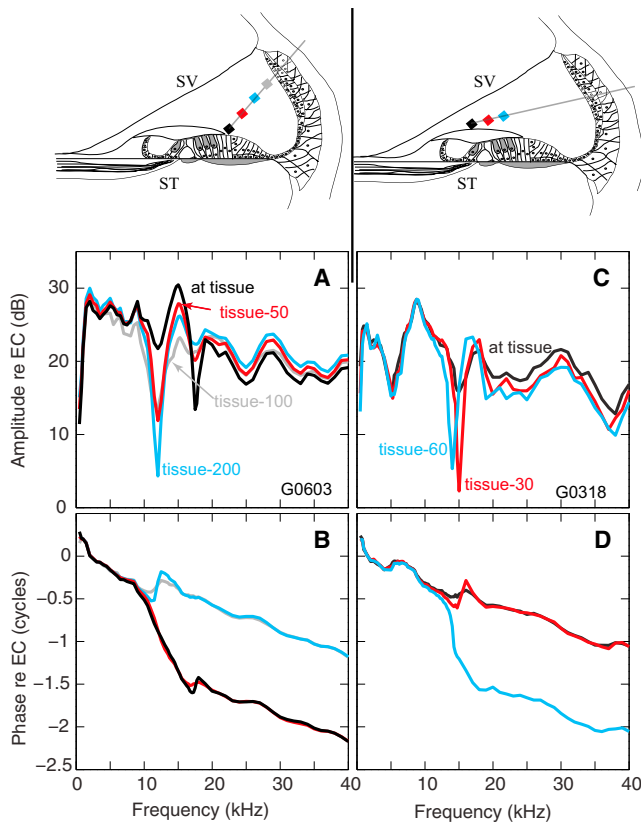
FIGURE 7   Variation in SM pressure in axial direction (G0603 and G0318). (*A* and *C*) SM pressure amplitude relative to ear canal pressure. (*B* and *D*) SM pressure phase relative to ear canal phase. Black curves were close to the tissue and the colored curves retracted the distances indicated in the labels. Estimated sensor tip location along direction of the sensor approach is shown by squares in cochlear sketches. To see this figure in color, go online.

the TM moved less at the more medial location than it did further lateral.

DISCUSSION

Notches in SM pressure—comparison with previous studies

Fig. 8 compares our SM data with Reissner's membrane motion measured in the apex of guinea pigs (9). The motion data look remarkably similar to our SM pressure measurements from the base. Cooper and Rhode later interpreted the notches they measured to be artifacts of a cochleostomy in the apical region (31). The cochleostomy allowed for a pressure release for the fast mode and led to fast-mode-induced fluid motion, leading to motion of the Reissner's membrane. In contrast, the notches that we observe in the pressure are a natural interaction between two pressure modes that exist even in an intact cochlea. The fact that Cooper and Rhode observed motion patterns very similar to our pressure data supports the two-mode interaction that they proposed to interpret their data and that we have further unraveled in these pressure measurements.
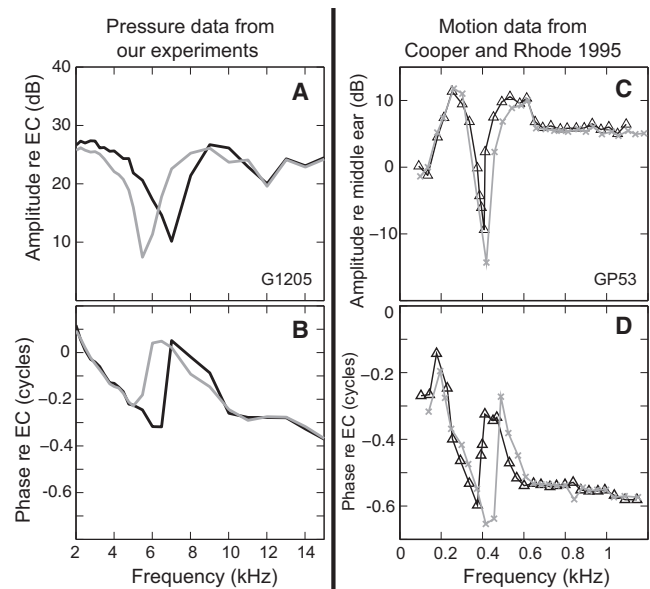
FIGURE 8   (*A* and *B*) SM pressure from one of our experiments compared with (*C* and *D*) Reissner's membrane motion measurement from the apex of a guinea pig (9).

Calculation of fast and slow modes

Because the SM and ST pressures were measured from opposite sides of the BM but roughly at the same location, we could compute the pressure difference across the CP. Performing complex vector subtraction on the cross-CP pressure data cancels the symmetric fast-compressional mode in the two scalae and leaves the antisymmetric mode, which contains both slow (TW) and fast-evanescent modes. As long as the slow mode dominates the evanescent mode, this is an estimate of the slow mode: $P_{antisymm} = (P_{SM} - P_{ST})/2 \sim P_{slow}$. Complex vector addition cancels the antisymmetric mode and leaves the symmetric mode, which is the fast-compressional mode: $P_{symm} = P_{fast-comp} = (P_{SM} + P_{ST})/2$ (*gray lines* in Fig. 9). Fig. 9, *A* and *B*, show $P_{antisymm} \sim P_{slow}$ computed from the data shown in Fig. 6, *A* and *B*. Fig. 9, *C* and *D*, and E and F, both show $P_{antisymm} \sim P_{slow}$ computed from the data shown in Fig. 6, *C* and *D*. The calibration uncertainty mentioned previously has a substantial effect on the subtraction and to better understand the results we did the subtraction in two different ways. First way: For the computation shown in Fig. 9, *A* and *B*, we shifted the ST pressure (shown in Fig. 6 *A*) down by an amount equal to the difference in mean ST pressure and mean SM pressure at frequencies above 18 kHz. Similarly, in Fig. 9, *C* and *D*, ST pressure was shifted up by an amount equal to the difference in mean ST and SM pressure above 18 kHz. This first way makes an assumption that above the peak the antisymmetric pressure mode is small, i.e., that the evanescent mode is small. This was a frequency-independent shift, to account for possible calibration error in the sensors. Second way: For the computation
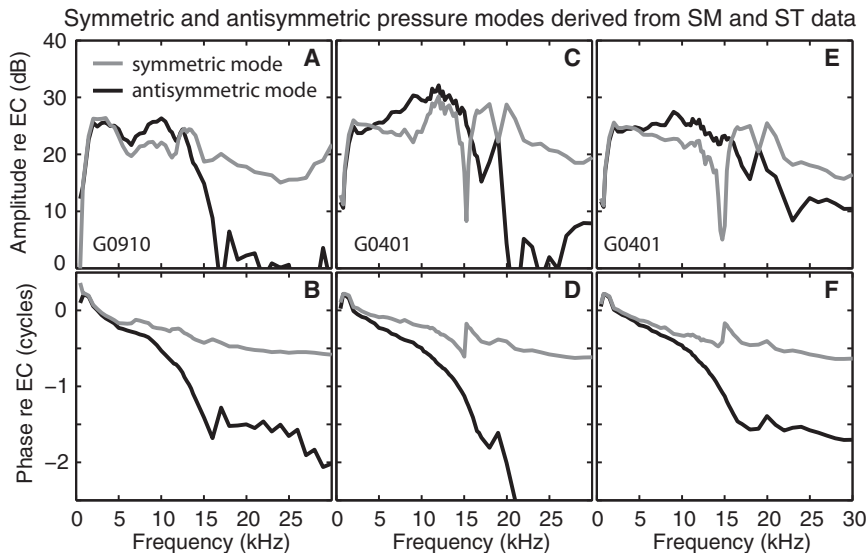
FIGURE 9 Antisymmetric mode (composed primarily of slow mode, also evanescent mode) and symmetric mode (fast-compressional mode) derived from SM and ST pressure in Fig. 6. (*A*) and (*B*) are from G0910 (Fig. 6, *A* and *B*). (*C*) and (*D*) are from G0401 (Fig 6, *C* and *D*). (*E*) and (*F*) are also from G0401 (Fig. 6, *C* and *D*), with the analysis done in a different way (see text for details).

shown in Fig. 9, *E* and *F*, the data from Fig. 6, *C* and *D*, were used without any shifting. This method does not do any calibration correction, and allows for the possibility that a more substantial evanescent mode exists. Much of our data indicated the presence of a significant evanescent mode, because the high-frequency plateau magnitude in SM (or SV) was usually greater than in ST. The evanescent pressure mode is certainly present at some level, because fast-mode responses that are too large to be due to compression are evident in BM motion (5,8,21) and fast-mode responses are also present in auditory nerve responses (32) and cochlear microphonic (33).

The decomposition into slow and fast modes requires pressure to be measured close to the sensory tissue, because the slow mode decays rapidly with distance from the tissue (34). The data presented here provide the most direct analysis of cochlear slow and fast modes to date. Dancer and Frank (35) did an early analysis based on pressure measured far from the sensory tissue, and Olson (19,28), did an analysis based on ST pressure at the sensory tissue and SV pressure far from the tissue.

In Fig. 9 *A*, $P_{symm} = P_{fast-comp}$ is almost flat with frequency and the corresponding phase delay of roughly 22 μs is attributable to middle ear delay (e.g., (36)). $P_{symm} = P_{fast-comp}$ in panels *C* and *E* is also quite flat but has pronounced notches. These occur when SM and ST pressures are out of phase and have the same amplitude (see Fig. 6). The only way to avoid notches in the symmetric mode is for the ST or SM pressure to be in a deep notch when they are out of phase. A slight misalignment of ST and SM sensors will throw that relationship off and lead to notches in the sum.

In Fig. 9, *A*–*D*, where the high-frequency plateau was used to normalize and correct for possible calibration error, $P_{antisymm} \sim P_{slow}$ has a sharp cutoff at ~15–20 kHz, dropping

over 20 dB. When the correction was not applied, in Fig. 9, *E* and *F*, the antisymmetric mode drop-off was less. In all cases, $P_{antisymm} \sim P_{slow}$ had a low-pass character, but in panel *E* it levels off at a new value that is higher than that in panel *C*. The antisymmetric mode phase showed TW phase accumulation through the low-pass region—thus, the low-pass region is the region of the slow mode. Above the cutoff frequency, both the amplitude and phase of the antisymmetric mode level off, and this is the region of the evanescent mode. The most important observation that emerges from the present analysis is that in the passive cochlea the slow, TW mode is low-pass in nature, a finding consistent with models of passive cochlear mechanics (2,10,37).

The analysis of Fig. 9 is a simple vector subtraction and addition, and is independent of a cochlear model. However, conceptually it is based in a two-compartment model, with a single partition, and the experimental results of Fig. 6 and the analytical extension of Fig. 9 are consistent with the predictions of a two-compartment, single-partition model. Conversely, the results are not consistent with models that predict substantially different TM and BM motions. However, this finding does not diminish the interest of two-partition models that allow for differences between the TM and BM motions. With fairly tight coupling between BM and TM, passive two-partition models predict rather subtle differences between BM (ST) and TM (SM) slow-waves (e.g., (16)). The resultant phase differences could give rise to interesting effects such as cochlear amplification activation, which has been both observed in experiments (30) and predicted by cochlear models (15). Thus, the two-partition models are key to understanding hair cell excitation, and the results here are a powerful informant of these models. The fact that we observed nearly antisymmetric slow-mode pressure in the two scalae (Fig. 6), suggests a

tight coupling between BM and TM. OCT measurements that measure motion within the CP also indicate that the TM (or more generally, the SM side of the OC) and the BM move quite similarly, although not in strict synchrony (17,38).

Expanding the analysis to active cochleae

Fig. 9 used the SM and ST data to calculate antisymmetric and symmetric modes, and thus analyze slow and fast modes. The calculation showed that the fast mode was, to first approximation, flat with frequency, with a delay that is attributed to middle ear. The slow mode was approximately low-pass, with a traveling wave delay + middle ear delay. In Fig. 10 we use these simple building blocks—fast and slow pressure modes, based on smoothed versions of Fig. 9, C and D,—to find SM and ST pressures. (For simplicity we take the evanescent mode to be zero, thus the antisymmetric mode is purely slow mode.) This is the reverse of the calculation for Fig. 9, and $P_{SM} = P_{fast} + P_{slow}$ and $P_{ST} = P_{fast} - P_{slow}$. Fig. 10, A and B, show the passive results—the fast (gray), slow (red), SM (blue), and ST (green) pressure. By construction, the calculated SM and ST pressures in panels A and B are much like our SM and ST data in Fig. 6, C and D, with similar peaks and notches. The SM and ST phases are offset by ~1/2 cycle through the region in which the ST pressure peaks. It is of particular interest that the ST pressure peak is much more pronounced than the nearly low-pass slow-mode pressure. This outcome of the model simulation further supports the idea that an approximately single-partition model—with tight coupling between BM and TM—describes passive cochlear mechanics.

Next, we extrapolate our findings, and use our knowledge of active ST pressure, to construct the pressure modes in an active cochlea. To proceed, note that based on ST pressure measured in active cochleae, the slow-mode is nonlinear, but the fast-mode is linear (5). This is sensible if the slow-mode is associated with CP motion and the fast-mode only with compression. Note that even in the case where there is fast-mode motion, it is observed to scale linearly (21). This is predicted in cochlear models that rely on the spatial variation in phasing of the TW for amplification (e.g., (13)). Here, we simply use the observation that the fast-mode is linear. Another observation from the literature that we use is that the phase of the slow-mode does not change much with level (19,21,39). Small phase changes do occur but to keep the analysis of Fig. 10 appropriately simple, we take the slow wave phase as level-independent (solid red line in Fig. 10 D). In Fig. 10, C and D, two active slow-mode pressures have been constructed (dotted and dashed red lines). The fast-mode pressure is unchanged from the passive case and not shown. The calculated active ST pressures are shown in the dotted and dashed green lines. In Fig. 10, E and F, active SM pressure is calculated (dotted and dashed blue lines). The ST pressure in the passive state (solid green line, Fig. 10 C) has the behavior we are used to seeing, with the deep notch at ~17 kHz (where the slow-mode has gone through 1.5 cycles relative to the fast-mode). When the slow mode is active this deep notch fades into a dimple, due to the dominance of the amplified slow mode over the fast mode (dotted green line in Fig. 10 C). A new ST notch has developed at ~21 kHz, where the slow-mode has gone through ~2.5 cycles relative to the fast-mode, and the amplified slow-mode is now large enough to interfere effectively with the fast-mode, producing a notch. The simulated active ST pressure was qualitatively similar to the active ST data in Fig. 3, particularly Fig. 3, C and D, and in the literature (19,30). These results
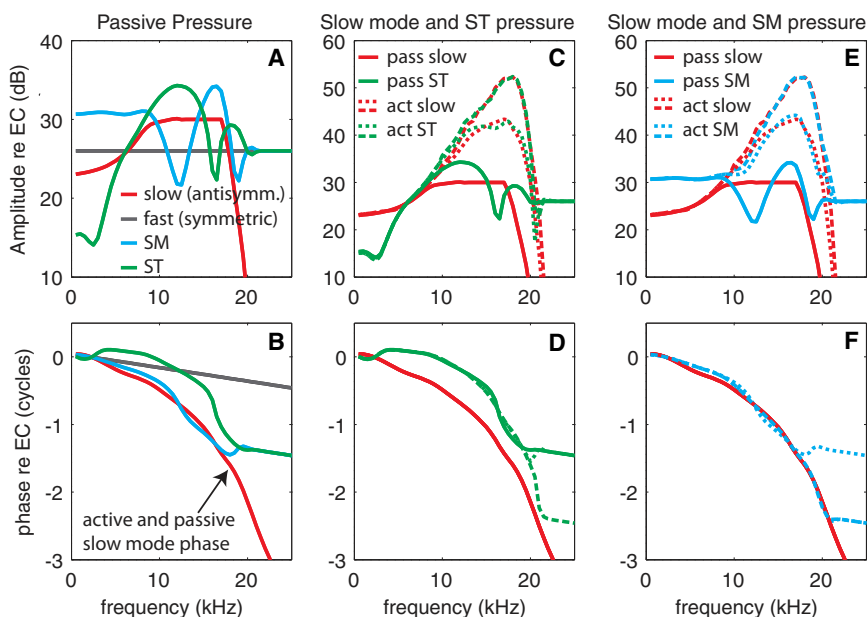
FIGURE 10 (A and B) Idealized versions of passive slow and fast mode pressures and predictions of passive SM and ST pressures. (C and D) Predictions of active slow mode and ST pressure (dashed and dotted lines) compared with passive slow mode and ST pressure (solid lines). (E and F) Predictions of active slow mode and SM pressure (dashed and dotted lines) compared with passive slow mode and SM pressure (solid lines). Passive slow and fast mode simulations were based on data shown in Fig. 9, C and D. To see this figure in color, go online.

support that both SM and ST pressure consist of underlying fast and slow pressure modes and that the passive TW slow-mode pressure is approximately low-pass in nature, as predicted by most models of passive cochlear mechanics. The predicted passive SM pressure (Fig. 10, *E* and *F*) (*solid blue line*), looks similar to much of the SM data presented here. The predicted SM pressure in the active state (*dotted and dashed blue lines*) looks quite similar to the active ST pressure (with a half-cycle phase difference), as would be expected when the slow-mode dominates the fast-mode.

CONCLUSION

This study provides the first, to our knowledge, experimental data set that directly explores the fluid-tissue interactions within the SM, and is the first, to our knowledge, study in which both SM and ST pressure were measured in the same cochlea. The results show a slow traveling wave pressure mode summing with a fast mode. The fast mode appeared to be primarily a compressional pressure with a smaller evanescent pressure mode adding. In the frequency region of slow mode dominance, SM and ST pressures at the sensory tissue were nearly antisymmetric, as predicted by classic, single-partition cochlear models. This finding is also consistent with the concept of a dual-partition model with relatively tight coupling between the two partitions (TM and BM). A second significant finding was that the passive slow mode is nearly low-pass in character. Extrapolating from our passive SM and ST findings and the tuned, nonlinear character of ST pressure in the active cochlea, the active slow mode and SM pressure are also tuned and nonlinear.

AUTHOR CONTRIBUTIONS

S.K. and E.S.O. contributed equally to designing and execution of experiments and manuscript preparation.

ACKNOWLEDGMENTS

REFERENCES

1. Von Békésy, G. 1980. Experiments in Hearing. R. E. Krieger Publishing, Melbourne, FL.

2. Siebert, W. M. 1974. Ranke revisited–a simple short-wave cochlear model. *J. Acoust. Soc. Am.* 56:594–600.

3. Peterson, L. C., and B. P. Bogart. 1950. A dynamical theory of the cochlea. *J. Acoust. Soc. Am.* 22:369–381.

4. Watts, L. 2000. The mode-coupling Liouville-Green approximation for a two-dimensional cochlear model. *J. Acoust. Soc. Am.* 108:2266–2271.

5. Olson, E. S. 2013. Fast waves, slow waves and cochlear excitation. *J. Acoust. Soc. Am.* 133:3508.

6. Steele, C. R., N. Kim, and S. Puria. 2008. Hook region represented in a cochlear model. *In* Concepts and Challenges in the Biophysics of Hearing. N. P. Cooper and D. T. Kemp, editors. World Scientific Publishing, Philadelphia, PA, pp. 323–329.

7. Taber, L. A., and C. R. Steele. 1981. Cochlear model including three-dimensional fluid and four modes of partition flexibility. *J. Acoust. Soc. Am.* 70:426–436.

8. Recio-Spinoso, A., and W. S. Rhode. 2015. Fast waves at the base of the cochlea. *PLoS One.* 10:e0129556.

9. Cooper, N. P., and W. S. Rhode. 1995. Nonlinear mechanics at the apex of the guinea-pig cochlea. *Hear. Res.* 82:225–243.

10. Kim, N., K. Homma, and S. Puria. 2011. Inertial bone conduction: symmetric and anti-symmetric components. *J. Assoc. Res. Otolaryngol.* 12:261–279.

11. Kolston, P. J. 2000. The importance of phase data and model dimensionality to cochlear mechanics. *Hear. Res.* 145:25–36.

12. Meaud, J., and K. Grosh. 2012. Response to a pure tone in a nonlinear mechanical-electrical-acoustical model of the cochlea. *Biophys. J.* 102:1237–1246.

13. Yoon, Y.-J., S. Puria, and C. R. Steele. 2007. Intracochlear pressure and derived quantities from a three-dimensional model. *J. Acoust. Soc. Am.* 122:952–966.

14. Lamb, J. S., and R. S. Chadwick. 2011. Dual traveling waves in an inner ear model with two degrees of freedom. *Phys. Rev. Lett.* 107:088101.

15. Lamb, J. S., and R. S. Chadwick. 2014. Phase of shear vibrations within cochlear partition leads to activation of the cochlear amplifier. *PLoS One.* 9:e85969.

16. Cormack, J., Y. Liu, …, S. M. Gracewski. 2015. Two-compartment passive frequency domain cochlea model allowing independent fluid coupling to the tectorial and basilar membranes. *J. Acoust. Soc. Am.* 137:1117–1125.

17. Lee, H. Y., P. D. Raphael, …, J. S. Oghalai. 2015. Noninvasive in vivo imaging reveals differences between tectorial membrane and basilar membrane traveling waves in the mouse cochlea. *Proc. Natl. Acad. Sci. USA.* 112:3128–3133.

18. Ghaffari, R., A. J. Aranyosi, and D. M. Freeman. 2007. Longitudinally propagating traveling waves of the mammalian tectorial membrane. *Proc. Natl. Acad. Sci. USA.* 104:16510–16515.

19. Olson, E. S. 2001. Intracochlear pressure measurements related to cochlear tuning. *J. Acoust. Soc. Am.* 110:349–367.

20. Dong, W., and E. S. Olson. 2008. Supporting evidence for reverse cochlear traveling waves. *J. Acoust. Soc. Am.* 123:222–240.

21. Rhode, W. S. 2007. Basilar membrane mechanics in the 6-9 kHz region of sensitive chinchilla cochleae. *J. Acoust. Soc. Am.* 121:2792–2804.

22. Rhode, W. S., and A. Recio. 2000. Study of mechanical motions in the basal region of the chinchilla cochlea. *J. Acoust. Soc. Am.* 107:3317–3332.

23. Robles, L., M. A. Ruggero, and N. C. Rich. 1986. Basilar membrane mechanics at the base of the chinchilla cochlea. I. Input-output functions, tuning curves, and response phases. *J. Acoust. Soc. Am.* 80:1364–1374.

24. Cooper, N. P. 1999. An improved heterodyne laser interferometer for use in studies of cochlear mechanics. *J. Neurosci. Methods.* 88:93–102.

25. Cooper, N. P. 1999. Radial variation in the vibrations of the cochlear partition. Proceedings of the International Symposium on Recent Developments in Auditory Mechanics. H. Wada, T. I. K. Takasaka, K. Ohyama, and T. Koike, editors. World Scientific, Sendai, Japan. 109–115.

26. Kohllöffel, L. U. E. 1973. Observations of the mechanical disturbances along the basilar membrane with laser illumination. *In* Basic Mechanisms in Hearing. A. Moller, editor. Elsevier, pp. 95–117.

27. Olson, E. S., and H. H. Nakajima. 2015. A family of fiber-optic based pressure sensors for intracochlear measurements. B. Choi, N. Kollias, H. Zeng, H. W. Kang, B. J. F. Wong, J. F. Ilgner, A. Nuttal, C.-P. Richter, M. C. Skala, M. W. Dewhirst, G. J. Tearney, K. W. Gregory, L. Marcu, A. Mandelis, and M. D. Morris, editors. SPIE BiOS. International Society for Optics and Photonics.

28. Olson, E. S. 1998. Observing middle and inner ear mechanics with novel intracochlear pressure sensors. *J. Acoust. Soc. Am.* 103:3445–3463.

29. de la Rochefoucauld, O., W. F. Decraemer, …, E. S. Olson. 2008. Simultaneous measurements of ossicular velocity and intracochlear pressure leading to the cochlear input impedance in gerbil. *J. Assoc. Res. Otolaryngol.* 9:161–177.

30. Dong, W., and E. S. Olson. 2013. Detection of cochlear amplification and its activation. *Biophys. J.* 105:1067–1078.

31. Cooper, N. P., and W. S. Rhode. 1996. Fast traveling waves, slow traveling waves, and their interactions in experimental studies of apical cochlear mechanics. *Aud. Neurosci.* 2:207–212.

32. Huang, S., and E. S. Olson. 2011. Auditory nerve excitation via a non-traveling wave mode of basilar membrane motion. *J. Assoc. Res. Otolaryngol.* 12:559–575.

33. Schmiedt, R. A., and J. J. Zwislocki. 1977. Comparison of sound-transmission and cochlear-microphonic characteristics in Mongolian gerbil and guinea pig. *J. Acoust. Soc. Am.* 61:133–149.

34. Olson, E. S. 1999. Direct measurement of intra-cochlear pressure waves. *Nature.* 402:526–529.

35. Dancer, A., and R. Franke. 1980. Intracochlear sound pressure measurements in guinea pigs. *Hear. Res.* 2:191–205.

36. de La Rochefoucauld, O., P. Kachroo, and E. S. Olson. 2010. Ossicular motion related to middle ear transmission delay in gerbil. *Hear. Res.* 270:158–172.

37. Steele, C. R., and K. M. Lim. 1999. Cochlear model with three-dimensional fluid, inner sulcus and feed-forward mechanism. *Audiol. Neuro-otol.* 4:197–203.

38. Chen, F., D. Zha, …, A. L. Nuttall. 2011. A differentially amplified motion in the ear for near-threshold sound detection. *Nat. Neurosci.* 14:770–774.

39. Versteegh, C. P. C., and M. van der Heijden. 2012. Basilar membrane responses to tones and tone complexes: nonlinear effects of stimulus intensity. *J. Assoc. Res. Otolaryngol.* 13:785–798.